Rifaximin prevents ethanol-induced liver injury in obese KK-A^{y} mice through modulation of small intestinal microbiota signature

Ryuta Kitagawa[1)], Kazuyoshi Kon[1)], Akira Uchiyama[1)], Kumiko Arai[1)], Shunhei Yamashina[1)], Kyoko Kuwahara-Arai[2)], Teruo Kirikae[2)], Takashi Ueno[3)], and Kenichi Ikejima[1)]

1) Department of Gastroenterology, 2) Department of Microbiology, 3) Laboratory of Proteomics and Medical Science, Research Support Center, Juntendo University Graduate School of Medicine,

2-1-1 Hongo, Bunkyo-ku, Tokyo, 113-8421 Japan

Short title: Rifaximin prevents ethanol-induced liver injury

Corresponding author:
Kazuyoshi Kon, MD, PhD, FAASLD
2-1-1 Hongo, Bunkyo-ku
Tokyo, 113-8421 Japan
Phone: +81-3-3813-3111, Fax: +81-3-3813-8862

E-mail: kazukon@juntendo.ac.jp

Abstract

Exacerbation of alcoholic hepatitis (AH) with comorbid metabolic syndrome is an emerging clinical problem, where microbiota plays a profound role in the pathogenesis. Here, we investigated the effect of rifaximin (RFX) on liver injury following chronic-binge ethanol (EtOH) administration in KK-A^y mice, a rodent model of metabolic syndrome. Female, 8-week-old KK-A^y mice were fed Lieber–DeCarli diet (5% EtOH) for 10 days, following a single EtOH gavage (4 g/kg BW). Some mice were given RFX (0.1 g/L, in liquid diet) orally. Small intestinal contents were collected from mice without binge. Intestinal microbiota was quantified using conventional, aerobic and anaerobic culturing techniques, and further analyzed by 16S rRNA sequencing in detail. EtOH-feeding/binge caused hepatic steatosis, oxidative stress, and induction of inflammatory cytokines in KK-A^y mice, which were markedly prevented by RFX treatment. Hepatic mRNA levels for cluster of differentiation (CD)-14, toll-like receptor (TLR) 4, TLR2 and NADPH oxidase (NOX) 2 were increased following EtOH-feeding/binge, and administration of RFX completely suppressed their increase. The net amount of small intestinal bacteria was increased over 3-fold after chronic EtOH feeding as expected; however, RFX did not prevent this net increase. Intriguingly, the profile of small intestinal microbiota was dramatically changed following EtOH

feeding in the order level, where the *Erysipelotrichales* predominated in the relative abundance. In sharp contrast, RFX drastically blunted the EtOH-induced increases in the *Erysipelotrichales* almost completely, with increased proportion of the *Bacteroidales*. In conclusion, RFX prevents AH through modulation of small intestinal microbiota/innate immune responses in obese KK-A^y mice.

NEW & NOTEWORTHY

Here we demonstrated that rifaximin (RFX) prevents chronic-binge ethanol (EtOH)-induced steatohepatitis in KK-A^y mice. Chronic EtOH feeding caused small intestinal bacterial overgrowth, with drastic alteration in the microbiota profile predominating the order Erysipelotrichales. RFX minimized this EtOH-induction in Erysipelotrichales with substitutive increases in Bacteroidales. RFX also prevented EtOH-induced increases in portal lipopolysaccaride, and hepatic cluster of differentiation (CD)-14, toll like receptor (TLR) 2 and TLR4 mRNA levels, suggesting the potential involvement of microbiota-related innate immune responses.

Keywords: alcoholic liver disease; toll-like receptor; pathogen-associated molecular patterns; metabolic syndrome; dysbiosis

Conflict of interest: No potential conflicts of interest were disclosed.

Financial support: This work was supported in part by JSPS KAKENHI (17K09440 to K.K. and 15K09023 to K.I.)

INTRODUCTION

The increasing mortality from alcoholic liver disease (ALD) has become one of the most serious health problems worldwide. Alcoholic hepatitis (AH) often occurs in patients who have a background of chronic drinking and a history of recent excessive drinking (3, 39). The treatment of AH is still largely dependent on corticosteroids, and no great progress has been made in the past 40 years (16). Patients with severe AH have a poor prognosis, with short-term mortality rates ranging from 30% to 40% (1, 36). Recently, the comorbidity of ALD and metabolic syndrome has become an emerging clinical problem worldwide (45). Indeed, epidemiological studies have suggested that metabolic syndrome increases the risk of alcoholic liver injury and related mortality, compared to alcohol alone (2, 44, 49).

From the pathophysiological point of view, ethanol (EtOH)-induced activation of liver innate immunity is one of the key events in the pathogenesis of ALD (10, 11, 53). Chronic alcohol exposure causes small intestinal bacterial overgrowth, induces qualitative alterations of gut flora, and compromises gut barrier function leading to elevation of intestinal permeability, thereby translocating bacterial products from gut to portal vein (33, 41, 60, 63). Common microbial patterns known as pathogen-associated molecular patterns (PAMPs) activate multiple downstream signaling pathways that

result in the synthesis of inflammatory cytokines in ALD (12). On the other hand, patients with metabolic syndrome also presented dysbiosis, and high-fat diet-induced obese mice showed intestinal permeability (8, 17). These findings suggested that there is a common background between AH and metabolic syndrome.

Recently, short-term chronic EtOH feeding combined with a single EtOH binge (Chronic-plus-Binge EtOH model or the NIAAA model) was proposed. This model shows significant serum alanine aminotransferase (ALT) elevation, fat accumulation, neutrophil infiltration in the liver, mimicking acute-on-chronic alcoholic liver injury in humans; however, pathological changes appear to be mild (5). KK-A^y mice are a congenic strain in which the A^y allele at the agouti locus had been transferred to the inbred KK strain by repetitive backcrossing. KK-A^y mice are a suitable model of steatohepatitis with metabolic syndrome, because they spontaneously become obese and develop hyperglycemia, hyperinsulinemia, and steatohepatitis (28, 55, 62). We have recently reported that NIAAA model using KK-A^y mice exhibits more prominent steatohepatitis than in C57BL/6 mice. These mice maintained the phenotype of obesity and hyperglycemia even under EtOH exposure; thus, the established animal model is considered to be useful as a model of alcoholic liver injury with a background of obesity and hyperglycemia (54).

99 Rifaximin (RFX), an oral non-absorbed antibiotic with broad-spectrum activity
100 against both Gram-positive and -negative aerobic and anaerobic bacteria, is widely used
101 for the prevention of hepatic encephalopathy. Additionally, several studies have reported
102 that the treatment with RFX ameliorated liver dysfunction and improved the prognosis
103 in cirrhotic patients (4, 23, 61). However, the effect of RFX on AH is unknown. In the
104 present study, therefore, we investigated the effect of RFX on chronic-binge-alcoholic
105 liver injury in KK-A^y mouse-used NIAAA model, focusing on the profile of small
106 intestinal microbiota.
107

Materials and Methods

Materials

The Liber–DeCarli liquid diet was purchased from Dyets (Bethlehem, PA). Anti-4-hydroxy-2-nonenal (4-HNE) primary antibody and anti-cytochrome P450 (CYP) 2E1 antibody were purchased from Abcam (Cambridge, MA). Anti-glyceraldehyde 3-phosphate dehydrogenase (GAPDH) was purchased from Cell Signaling Technology (Danvers, MA). Biotinylated anti-mouse IgG antibody was purchased from Santa Cruz Biotechnology (Dallas, TX). All other reagents were purchased from Sigma unless otherwise specified (St.Louis, MO).

Animals and experimental design

All experimental protocols were approved by the Committee of Laboratory Animals following the institutional guidelines. Animals were housed in air-conditioned, specific pathogen-free animal quarters, with lighting from 0800 to 2000 h. The mice were given unrestricted access to standard laboratory chow and water until the study began. All mice were kept separately in single cages. At 8 weeks of age and after acclimation, female KK-A^y mice (CLEA Japan, Tokyo, Japan) were fed Lieber–DeCarli liquid diet containing 5% EtOH, or pair-fed control diet containing isocaloric

maltodextrin for 10 days. Some mice were given RFX (0.1 g/L) in the liquid diet during the feeding period. Feeding tubes containing ethanol or a control liquid diet were replaced daily at late afternoon. On day 11, animals received a single gavage of 24% EtOH (4 g/kg BW) or isocaloric maltodextrin between 7:00 am and 9:00 am, and then were euthanized 6 h later by inhalation of isoflurane mixed with oxygen and air; liver tissues and portal/inferior vena caval blood samples were collected. Some mice were euthanized without binge for collecting of small intestinal contents. The liver tissues and small intestinal contents were kept frozen at -80ºC until analysis.

Serum transaminase level

The levels of ALT and triglyceride (TG) in serum from inferior vena cava (IVC) were measured colorimetrically using the Fuji DRI-CHEM system (Fuji Film Medical Co. Ltd., Tokyo, Japan).

Histological analysis and immunohistochemistry

For histological evaluations, liver tissues were fixed in 10 % buffered formalin, embedded in paraffin, and stained with Hematoxylin and Eosin (H&E). For Oil Red O staining, liver tissues frozen in OCT compounds were used. The expression and

144 localization of tissue 4-HNE in the liver was detected by immunohistochemical staining
145 as previously described elsewhere (29). Briefly, deparaffinized tissue sections were
146 incubated with a monoclonal anti-4-HNE antibody and secondary biotinylated
147 anti-mouse IgG, and the specific binding was visualized with the avidin-biotin complex
148 solution followed by incubation with a 3,3-diaminobenzidine tetrahydrochloride
149 solution using Vectastain Elite ABC kit (Vector Laboratories, Burlingame, CA).
150 Specimens for histology and immunohistochemistry were observed under an optical
151 microscope (DM7000; Leica, Wetzlar, Germany) equipped with a digital microscope
152 camera (MC120HD; Leica, Wetzlar, Germany). We evaluated the antibody qualitatively
153 by using sections treated without antibody as negative control and using liver tissue
154 collected from mice treated with acetaminophen as positive control.
155
156 *Triacylglycerol assay*
157 Triacylglycerol concentration in liver tissue was determined colorimetrically as
158 previously described (54).
159
160 *RNA preparation and real-time reverse transcription polymerase chain reaction*
161 *(RT-PCR)*

Total RNA was prepared from frozen tissue samples using the illustra RNAspin Mini RNA Isolation kit (GE healthcare, Waukesha, WI). The concentration and purity of the isolated RNA were then determined by measuring the optical density at 260 and 280 nm. For real-time RT-PCR, total RNA (1 μg) was reverse transcribed using Moloney murine leukemia virus transcriptase (SuperScript II; Invitrogen, Carlsbad, CA) and an oligo (dT) 12–18 primer at 42 °C for 1 h. The obtained cDNA (1 μg) was then amplified using Fast SYBR Green Master Mix (Applied Biosystems, Foster City, CA) and specific primers for acetyl-CoA carboxylase α (ACCα), fatty acid synthase (FAS), tumor necrosis factor α (TNFα), interleukin 6 (IL6), interferon γ (IFNγ), chemokine (C-C motif) ligand 2 (CCL2), toll like receptor (TLR) 2, TLR4, cluster of differentiation (CD)-14, heme oxygenase 1 (HO1), NADPH oxidase (NOX) 1, NOX2 and GAPDH (Table 1).

Measurement of LPS levels in portal vein

To measure lipopolysaccharide (LPS) in blood samples from portal vein ,the Hycult Biotech Limulus Amebocyte Lysate assay (Hycult Biotech, Uden, the Netherlands) was used according to the manufacturer's directions.

Measurement of gut permeability

D-xylose solution (5% (w/v), 100 μL/mice) was gavaged on day 11 with EtOH (4 g/kg BW) or isocaloric maltodextrin, and then animals were euthanized 2 h later by inhalation of isoflurane mixed with oxygen and air; liver and serum samples were collected. Plasma D-xylose concentration was measured using D-Xylose Assay (Chondrex. Inc., Redmond, WA) according to the manufacturer's directions.

Western blot analysis

Protein extracts (20 μg) were electrophoresed in 10 % sodium dodecyl sulfate (SDS) polyacrylamide gels and electrophoretically transferred onto polyvinylidene fluoride membranes. The membranes were then blocked with Bullet Blocking One for Western Blotting (NACALAI TESQUE, Kyoto, Japan) and incubated with primary antibodies against CYP2E1 (anti-rabbit, 1:1000), and GAPDH (anti-rabbit, 1:1000), followed by a secondary horseradish peroxidase-conjugated anti-rabbit IgG antibody. Specific bands were then visualized using the ECL prime detection kit (GE healthcare, Waukesha, WI) and detected using a Fusion FX7 imaging system (Vilber Lourmat, Torcy, France).

198 *CYP2E1 activity assay*

199 CYP2E1 activity was determined with liver homogenates using p-nitrophenol as a
200 substrate, according to a previously described procedure (54) .

201

202 *Bacterial colony count*

203 Fresh small intestinal contents were immediately weighed, dissociated in liquid
204 thioglycolate media (Sigma) and diluted 1:10000 prior to plating onto sheep blood agar
205 (Nissui Plate Sheep Blood Agar; Nissui, Tokyo, Japan) under aerobic or anaerobic
206 conditions on the same day. Plates were incubated at 37ºC for 24h. The net amount of
207 viable bacterial cells was expressed as colony forming units (CFU) / g counted and
208 normalized to the mass of small intestinal contents.

209

210 *16S rRNA sequencing*

211 Small intestinal contents were frozen at -80°C. The microbial DNA was
212 extracted using the Isospin fecal DNA (NIPPON GENE Co. Ltd., Tokyo, Japan). The
213 V1V2 regions of 16S rRNA genes were amplified and sequenced by MiSeq Deep
214 sequencer using MiSeq Reagent Kit v3 (Illumina, San Diego, CA) following
215 manufacturer's instruction. The sequence data was preprocessed and analyzed using the

"Flora Genesis software" (Repertoire Genesis, Ibaraki, Japan). In brief, the R1 and R2 read pairs were joined and chimera sequences were removed. The operational taxonomic unit (OTU) picking was performed by the open-reference method using the 97% ID prefiltered Greengenes database and the uclust. The representative sequences of each OTUs were picked and taxonomy assignment was performed by Ribosomal Database Project (RDP) classifier using its threshold score 0.5 or more. The OTUs were grouped if their annotation was same regardless its RDP score. Sequencing of partial 16S RNA genes was performed by Repertoire Genesis.

Statistical analysis

Morphometric and densitometric analyses were performed using Scion Image (ver. Beta 4.0.2, Scion Corp., Fredrick, MD). Data were expressed as means ± SEM. Statistical differences between means were determined using one way analysis of variance (ANOVA) on ranks followed by an all pairwise multiple comparison procedure (Student-Newman-Keuls Method) as appropriate. $P < 0.05$ was selected before the study to reflect significance.

Results

RFX ameliorates hepatic steatosis and inflammation caused by chronic-binge EtOH feeding

Food intake and changes of body weight during the experimental period showed no significant difference among each group (Fig. 1, *A* and *B*). Serum ALT levels at 6 h after EtOH binge were significantly elevated to 229 ± 14 IU/L, compared with the values of 41 ± 5 IU/L in controls; treatment with RFX significantly blunted the increase to 95 ± 10 IU/L (Fig. 1C, $P < 0.05$). Serum TG levels were also raised more than 3 times that in the EtOH group and were significantly suppressed by RFX administration (Fig. 1D, $P < 0.05$). Livers from EtOH group were enlarged with diffuse yellowish tone, which indicated severe steatosis; which were clearly reduced by RFX (Fig. 1E). The liver/body weight ratio at 6 h after EtOH binge was significantly higher than controls with isocaloric dextrin gavage; whereas treatment with RFX prevented the increase almost completely (Fig. 1*F*, $P < 0.05$).

Liver histology showed that chronic-binge EtOH-feeding induced overt hepatic steatosis around the central veins 6 h after EtOH binge; however, treatment with RFX significantly prevented the pathological findings. Oil Red O staining performed to confirm the distribution of lipid droplets on liver tissue revealed that the livers of

KK-A^y mice have lipid droplets throughout the liver lobules, even in the control group. As expected, a large amount of fat droplets appeared to fill up the entire hepatic lobule in the EtOH group, and RFX remarkably reduced it (Fig. 2*A*). The measurement of lipids extracted from liver further confirmed the significant increase of hepatic TG by EtOH and the suppressive effect of TG by RFX (Fig. 2*B*, $p<0.05$). Whereas the hepatic expression levels of mRNA for ACCα and FAS, genes promoting lipogenesis, were significantly increased in chronic-binge EtOH-fed mice, the treatment with RFX inhibited both of the expression to basal levels (Fig. 2*C and D*, $p<0.05$). In contrast, the expression of CPT1A, the rate-limiting enzyme of fatty acid β-oxidation, was reduced to 56 ± 2% of control by EtOH administration, which improved to 97 ± 6% by RFX (Fig. 2E, $p<0.05$).

RFX decreases overexpression of inflammatory cytokines in the liver in chronic-binge EtOH-fed mice.

The hepatic expression levels of mRNA for TNFα, IL6, inflammatory cytokines, were significantly increased in chronic-binge EtOH-fed mice as expected, whereas treatment with RFX blunted these expressions significantly (Fig. 3, *A* and *B*, $P < 0.05$). The expression of IFNγ, which is secreted by activated T cells and natural killer cells

and enhances macrophages, was also increased in chronic-binge EtOH. Additionally, the expression of a macrophage-tropic chemokine CCL2 was markedly enhanced in EtOH group. RFX completely reduced the expression of IFNγ to the basal levels and significantly decreased CCL2 (Fig. 3*C* and *D*, $p<0.05$). The hepatic mRNA expression for CD-14, the co-receptor for TLR4 and TLR2, was increased in chronic-binge EtOH-fed mice compared with controls; treatment with RFX significantly blunted the mRNA expression (Fig. 3*E*, $P < 0.05$). The hepatic expression of mRNA for TLR4 and TLR2 significantly increased in chronic-binge EtOH-fed mice compared with controls, and RFX significantly blunted the mRNA expression both of TLR4 and 2 (Fig. 3*F* and *G*, $P < 0.05$). LPS in portal vein blood was more than doubled by chronic-binge EtOH and was almost completely suppressed by RFX (Fig. 3*H*, $P < 0.05$). In contrast, D-xylose absorption assay showed no effect of RFX on gut permeability increased by chronic-binge EtOH (Fig. 3I).

RFX prevents oxidative stress induced by chronic-binge EtOH

Oxidative stress in hepatocytes after chronic-binge EtOH feeding was evaluated by immunohistochemical staining of 4-HNE. This assay revealed that chronic-binge EtOH significantly increased the 4-HNE-positive area to 22.8 ± 2.3%, compared with

287 values of 12.5 ± 2.4% in controls; treatment with RFX significantly reduced the
288 4-HNE-positive area to 16.7 ± 1.1% (Fig. 4, *A*, $P < 0.05$). The hepatic expression of
289 HO1 mRNA, another oxidative stress marker in the liver, was measured by qPCR. The
290 hepatic expression levels of HO1 mRNA were significantly increased in chronic-binge
291 EtOH-fed mice compared with controls. Treatment with RFX significantly blunted the
292 mRNA expression (Fig. 4*C* $P < 0.05$). The hepatic expression of NOX1 and 2 was also
293 measured by qPCR. Whereas the expression of NOX1 did not show significant change
294 by chronic-binge EtOH, the expression of NOX2 was significantly increased by
295 chronic-binge EtOH. The treatment with RFX significantly prevented the NOX2 mRNA
296 expression (Fig. 4*D* and *E, P<0.05*). CYP2E1 was measured by western blotting using
297 GADPH as a normalization standard. CYP2E1 significantly increased after
298 chronic-binge EtOH feeding compared with the controls; treatment with RFX had no
299 effect on this increase (Fig. 4*F,* $P < 0.05$). Additionally, chronic-binge EtOH-enhanced
300 CYP2E1 activity was not either inhibited by RFX (Fig. 4*G*).
301
302 *RFX has no effect on the net amount of viable bacterial cells increased by chronic EtOH*
303 *feeding.*
304 The net amount of viable aerobic and anaerobic bacterial cells in small intestine

dramatically increased after chronic EtOH feeding compared with controls. Treatment with RFX showed no significant difference compared with EtOH-fed group (Fig. 5, *A* and *B*, $P < 0.05$).

RFX induces taxonomic shifts in small intestinal bacterial communities in chronic EtOH-fed mice.

In the phyrum level, the profile of small intestinal microbiota following EtOH-feeding showed minimal changes compared with controls (Fig. 6*A*). However, the order *Lactobacillales*, which accounted for 51 ± 11 % in controls, drastically decreased to 2.8 ± 1.1 % in EtOH-fed group (Fig. 6, *B* and *C*, $P < 0.05$). Instead, the order *Erysipelotrichales* dramatically increased to 68 ± 1 % after EtOH-feeding, compared with values of 25.2 ± 5.0 % in controls (Fig. 6, *B* and *D*, $P < 0.05$). Treatment with RFX largely reversed the order *Erysipelotrichales* to 11 ± 2 % (Fig. 6, *B* and *D*, $P < 0.05$) and dramatically enriched the order *Bacteroidales* to 55 ± 6% (Fig. 6, *B* and *E*, $P < 0.05$).

Discussion

In the present study, the treatment with RFX prevented severe steatohepatitis around central veins caused by chronic-binge EtOH feeding in KK-A^y mice (Fig. 1*E* and 2*A*). RFX significantly blunted chronic-binge EtOH-induced increases in ACCα (Fig. 2*C*) and FAS (Fig. 2*D*), two major enzymes of the lipogenesis pathway. Further, and prevented decreases in CPT1A (Fig. 2*E*), indicating that RFX treatment in vivo reverts down-regulation of β-oxidation mostly caused by EtOH. These findings demonstorate that RFX treatment modify lipid metabolism in liver, thereby preventing hepatic steatosis caused by EtOH with comorbid metabolic syndrome.

Chronic and binge ethanol feeding elicits production of pro-inflammatory cytokines and chemokines, such as TNFα, IL6, IFNγ, and CCL2 in KK-A^y mouse liver as expected. However, RFX markedly downregulated these phenomenon (Fig. 3, *A*-*D*). Ethanol administration *in vivo* is associated with the formation of free radicals due to oxidant stress (25). RFX prevented oxidative stress in the liver following chronic-binge EtOH feeding, evidenced by the expressions of 4-HNE and mRNA for HO1 (Fig. 4*A*). HO-1 can be used as a oxidative stress marker because it is upregulated by oxidative stress, although it works as an antioxidant (24). It has been reported that chronic EtOH

feeding increases the LPS-stimulated NOXs-dependent production of reactive oxygen species (ROS) in Kupffer cells (31, 57). Particularly, NOXs play an important role in alcoholic steatohepatitis with a mechanism involving FASN and ACCα (34). In our study, RFX reduced oxidative stress possibly through the down regulation of NOX2, which is an isoform predominantly express on macrophages (Fig. 4*D* and *E*). Taken together, it is hypothesized that NOX2, mostly in hepatic macrophages, is the target of action of RFX in terms of enhanced hepatic oxidative stress caused by EtOH with comorbid metabolic syndrome.

CYP2E1 is induced predominantly in the hepatocytes by EtOH and could be a source of reactive oxygen species, leading to liver injury (51). However, some reports suggested that CYP2E1 plays only a small role in mechanisms of AH (30, 32). Taken together, the role of CYP2E1 in AH is controversial. Our data revealed that the EtOH-induction in hepatic protein levels and activity of CYP2E1 was not blunted by RFX (Fig. 3*F and G*), suggesting that the protective effect of RFX on chronic-binge EtOH-induced steatohepatitis was independent of CYP2E1-mediated EtOH metabolism.

TLRs are the main pattern recognition receptors on liver cells and have an

important role in detecting a variety of invading microorganisms and their products, and eliciting early innate immune responses (3, 36, 40). Activation of Kupffer cells via TLR4, a receptor for lipopolysaccharide produced by Gram-negative bacteria, is involved in the pathogenesis of alcohol-induced liver injury (18, 38, 59). The co-receptor CD-14 is required by TLR4 to response to microbial components, enhancing TLR4-mediated pro-inflammatory responses to bacterial pathogens (48). In our data, the prevention of overexpression of CD-14 and TLR4 mRNA by RFX indicates the suppressive effect against TLR4 signaling pathway after EtOH-feeding/binge (Fig. 3, *E* and *F*). On the other hand, TLR2 recognizes the surface molecules of Gram-positive bacteria such as lipoteichoic acid and peptidoglycan, potent stimulators of innate inflammatory responses (56). Recent studies have indicated that TLR2 is also related with the development of AH. Some reports indicated that chronic alcohol feeding increases hepatic expression levels for TLR2 (14, 26, 46), and chronic-binge EtOH-induced liver damage and inflammation are prevented in TLR2-deficient mice (50). We have measured the concentration of lipoteichoic acid and lipopolysaccharide (LPS) in the portal blood 6 hr after gavage of EtOH. Lipoteichoic acid in portal blood was not different between control and EtOH groups (data not shown) whereas LPS levels in the portal blood were significantly elevated in EtOH

group. This is consistent with previous reports indicating the role of gut-derived endotoxin in alcoholic and nonalcoholic steatohepatitis (47, 59); therefore, here we focused on LPS as the main bacterial product involved in our animal model. On the other hand, we evaluated gut permeability using D-xylose absorption test (Fig. 3I). As expected, D-xylose absorption is increased following chronic EtOH and binge, which was not prevented by RFX, indicating that RFX does not revert EtOH-induced leaky-gut in this model.

It has been reported that single administration of EtOH binge without chronic EtOH does not cause any liver damage in the chronic-binge EtOH model (5). In this study, therefore, we analyzed small intestinal contents prior to EtOH binge, considering that chronic changes in the intestinal flora due to alcohol intake may have a major effect on liver damage after EtOH binge. Chronic alcohol consumption induces small and large intestinal bacterial overgrowth and dysbiosis in animals and humans (6, 63). Our data also demonstrated that chronic EtOH exposure led to aerobic and anaerobic bacterial overgrowth in the small intestine (Fig. 5). Previous study showed that RFX administration caused no significant changes in principle component analysis, quantitative assessment of gut microbiota using multitag pyrosequencing, in fresh stool

393 in patients with cirrhosis (4). Our data derived from conventional culturing techniques
394 also indicated that RFX had no effect on the net amount of small intestinal viable
395 bacterial cells increased by chronic EtOH feeding (Fig. 5).
396
397 In patients with cirrhosis treated by RFX, the relative abundance of stool
398 pathogenic bacteria indicated only a slight change compared with before-treatment (21).
399 The present study demonstrated that chronic EtOH consumption dramatically modified
400 relative abundance of the small intestinal microbiota in KK-A^y mice, increasing the
401 relative abundance of the order *Erysipelotrichales* and decreasing the order
402 *Lactobacillales* compared with pair-fed control mice (Fig. 6, *B-D*). The order
403 *Erysipelotrichales* and *Lactobacillales* belong to the *Firmicutes* phylum. The order
404 *Erysipelotrichales*, Gram-positive facultative anaerobes, increased in canines with a diet
405 high in refined maize and low in fiber (15), in mice with high fat diets (37), in mouse
406 models of acute inflammatory colitis (52), in humans with Crohn's disease (13), and in
407 humans with obesity, western-type diets, and increased host cholesterol metabolite. The
408 involvement to host lipid metabolism has been considered as a mechanism by which the
409 *Erysipelotrichales* are related to each disease in human. (20). *Lactobacillales* is an order
410 of Gram-positive obligate anaerobes, which has been shown to prevent alcoholic liver

injury as probiotics (7, 43). The treatment of RFX dramatically modified the component of the small intestinal microbiota caused by chronic EtOH feeding, decreasing the relative abundance of the order *Erysipelotrichales* and increasing the order *Bacteroidales* (Fig. 6, *B*, *D*, and *E*). It also indicated that the treatment of RFX drastically decreased the *Firmicutes*/*Bacteroidetes* ratio of the small intestinal microbiota of KK-A^{y} mice (Fig. 5*A*). Since the order *Bacteroidales* is Gram-negative obligate anaerobes, the data of 16S rRNA here does not simply explain the fact that RFX reduced LPS in the portal blood by RFX. However, previous studies showed a decreased abundance of its family *Bacteroidaceae* in patients with liver cirrhosis, in particular in alcoholic cirrhosis (9, 22, 42). In addition, other studies have shown that *Firmicutes*/*Bacteroidetes* ratio was increased in obese mice and humans compared with lean individuals (27, 35, 58), and in human with short-term overnutrition (19). Taken together, the decrease of *Firmicutes*/*Bacteroidetes* ratio induced by RFX may have potential to prevent alcoholic liver injury.

In conclusion, our findings demonstrated that the treatment with RFX prevented alcoholic liver injury through suppressing inflammatory cytokines, chemokines and oxidative stress in obese KK-A^{y} mice. Furthermore, this study presented that RFX

429 dramatically modified the small intestinal microbiota following chronic EtOH feeding,
430 decreasing the relative abundance of the order Erysipelotrichales and increasing the
431 order Bacteroidales, without affecting EtOH-induced increase of net amount of viable
432 bacteria. These findings indicate that the RFX-induced modulation of small intestinal
433 microbiota plays a pivotal role to prevent alcoholic liver injury in this obese KK-A^y
434 mouse model. Modulation of microbiota by RFX is a promising approach for
435 prevention/treatment of AH.
436

437 **Acknowledgments**

438 The authors thank Takako Ikegami and Tomomi Ikeda (Laboratory of
439 Molecular and Biochemical Research, Research Support Center, Juntendo University
440 Graduate School of Medicine, Tokyo, Japan) for technical assistance.
441

References

1. EASL clinical practical guidelines: management of alcoholic liver disease. *J Hepatol* 57: 399-420, 2012.

2. **Almeda-Valdes P, Altamirano-Barrera A, Uribe M, and Mendez-Sanchez N**. Metabolic Features of Alcoholic Liver Disease. *Rev Recent Clin Trials* 11: 220-226, 2016.

3. **Altamirano J, and Bataller R**. Alcoholic liver disease: pathogenesis and new targets for therapy. *Nature Reviews Gastroenterology &Amp; Hepatology* 8: 491, 2011.

4. **Bajaj JS, Heuman DM, Sanyal AJ, Hylemon PB, Sterling RK, Stravitz RT, Fuchs M, Ridlon JM, Daita K, Monteith P, Noble NA, White MB, Fisher A, Sikaroodi M, Rangwala H, and Gillevet PM**. Modulation of the metabiome by rifaximin in patients with cirrhosis and minimal hepatic encephalopathy. *PLoS One* 8: e60042, 2013.

5. **Bertola A, Mathews S, Ki SH, Wang H, and Gao B**. Mouse model of chronic and binge ethanol feeding (the NIAAA model). *Nat Protoc* 8: 627-637, 2013.

6. **Bode JC, Bode C, Heidelbach R, Durr HK, and Martini GA**. Jejunal microflora in patients with chronic alcohol abuse. *Hepatogastroenterology* 31: 30-34, 1984.

7. **Bull-Otterson L, Feng W, Kirpich I, Wang Y, Qin X, Liu Y, Gobejishvili L, Joshi-Barve S, Ayvaz T, Petrosino J, Kong M, Barker D, McClain C, and Barve S**. Metagenomic analyses of alcohol induced pathogenic alterations in the intestinal microbiome and the effect of Lactobacillus rhamnosus GG treatment. *PLoS One* 8: e53028, 2013.

8. **Cani PD, Bibiloni R, Knauf C, Waget A, Neyrinck AM, Delzenne NM, and Burcelin R**. Changes in gut microbiota control metabolic endotoxemia-induced inflammation in high-fat diet-induced obesity and diabetes in mice. *Diabetes* 57: 1470-1481, 2008.

9. **Chen Y, Yang F, Lu H, Wang B, Chen Y, Lei D, Wang Y, Zhu B, and Li L**. Characterization of fecal microbial communities in patients with liver cirrhosis. *Hepatology* 54: 562-572, 2011.

10. **Cohen JI, and Nagy LE**. Pathogenesis of alcoholic liver disease: interactions between parenchymal and non-parenchymal cells. *J Dig Dis* 12: 3-9, 2011.

11. **Gao B, and Bataller R**. Alcoholic liver disease: pathogenesis and new therapeutic targets. *Gastroenterology* 141: 1572-1585, 2011.

12. **Gao B, Seki E, Brenner DA, Friedman S, Cohen JI, Nagy L, Szabo G, and Zakhari S**. Innate immunity in alcoholic liver disease. *Am J Physiol Gastrointest Liver*

Physiol 300: G516-525, 2011.

13. **Gevers D, Kugathasan S, Denson LA, Vazquez-Baeza Y, Van Treuren W, Ren B, Schwager E, Knights D, Song SJ, Yassour M, Morgan XC, Kostic AD, Luo C, Gonzalez A, McDonald D, Haberman Y, Walters T, Baker S, Rosh J, Stephens M, Heyman M, Markowitz J, Baldassano R, Griffiths A, Sylvester F, Mack D, Kim S, Crandall W, Hyams J, Huttenhower C, Knight R, and Xavier RJ**. The treatment-naive microbiome in new-onset Crohn's disease. *Cell Host Microbe* 15: 382-392, 2014.

14. **Gustot T, Lemmers A, Moreno C, Nagy N, Quertinmont E, Nicaise C, Franchimont D, Louis H, Deviere J, and Le Moine O**. Differential liver sensitization to toll-like receptor pathways in mice with alcoholic fatty liver. *Hepatology* 43: 989-1000, 2006.

15. **Hang I, Rinttila T, Zentek J, Kettunen A, Alaja S, Apajalahti J, Harmoinen J, de Vos WM, and Spillmann T**. Effect of high contents of dietary animal-derived protein or carbohydrates on canine faecal microbiota. *BMC Vet Res* 8: 90, 2012.

16. **Helman RA, Temko MH, Nye SW, and Fallon HJ**. Alcoholic hepatitis. Natural history and evaluation of prednisolone therapy. *Ann Intern Med* 74: 311-321,

1971.

17. **Holmes E, Kinross J, Gibson GR, Burcelin R, Jia W, Pettersson S, and Nicholson JK**. Therapeutic modulation of microbiota-host metabolic interactions. *Sci Transl Med* 4: 137rv136, 2012.

18. **Hritz I, Mandrekar P, Velayudham A, Catalano D, Dolganiuc A, Kodys K, Kurt-Jones E, and Szabo G**. The critical role of toll-like receptor (TLR) 4 in alcoholic liver disease is independent of the common TLR adapter MyD88. *Hepatology* 48: 1224-1231, 2008.

19. **Jumpertz R, Le DS, Turnbaugh PJ, Trinidad C, Bogardus C, Gordon JI, and Krakoff J**. Energy-balance studies reveal associations between gut microbes, caloric load, and nutrient absorption in humans. *Am J Clin Nutr* 94: 58-65, 2011.

20. **Kaakoush NO**. Insights into the Role of Erysipelotrichaceae in the Human Host. *Front Cell Infect Microbiol* 5: 84, 2015.

21. **Kaji K, Takaya H, Saikawa S, Furukawa M, Sato S, Kawaratani H, Kitade M, Moriya K, Namisaki T, Akahane T, Mitoro A, and Yoshiji H**. Rifaximin ameliorates hepatic encephalopathy and endotoxemia without affecting the gut microbiome diversity. *World J Gastroenterol* 23: 8355-8366, 2017.

22. **Kakiyama G, Hylemon PB, Zhou H, Pandak WM, Heuman DM, Kang DJ,**

514 **Takei H, Nittono H, Ridlon JM, Fuchs M, Gurley EC, Wang Y, Liu R, Sanyal AJ,**
515 **Gillevet PM, and Bajaj JS**. Colonic inflammation and secondary bile acids in
516 alcoholic cirrhosis. *Am J Physiol Gastrointest Liver Physiol* 306: G929-937, 2014.

517 23. **Kalambokis GN, and Tsianos EV**. Rifaximin reduces endotoxemia and
518 improves liver function and disease severity in patients with decompensated cirrhosis.
519 *Hepatology* 55: 655-656, 2012.

520 24. **Kamalvand G, Pinard G, and Ali-Khan Z**. Heme-oxygenase-1 response, a
521 marker of oxidative stress, in a mouse model of AA amyloidosis. *Amyloid* 10: 151-159,
522 2003.

523 25. **Kennedy SW, and Jones SP**. Simultaneous measurement of cytochrome
524 P4501A catalytic activity and total protein concentration with a fluorescence plate
525 reader. *Anal Biochem* 222: 217-223, 1994.

526 26. **Kirpich IA, Feng W, Wang Y, Liu Y, Barker DF, Barve SS, and McClain**
527 **CJ**. The type of dietary fat modulates intestinal tight junction integrity, gut permeability,
528 and hepatic toll-like receptor expression in a mouse model of alcoholic liver disease.
529 *Alcohol Clin Exp Res* 36: 835-846, 2012.

530 27. **Koliada A, Syzenko G, Moseiko V, Budovska L, Puchkov K, Perederiy V,**
531 **Gavalko Y, Dorofeyev A, Romanenko M, Tkach S, Sineok L, Lushchak O, and**

Vaiserman A. Association between body mass index and Firmicutes/Bacteroidetes ratio in an adult Ukrainian population. *BMC Microbiol* 17: 120, 2017.

28. **Kon K, Ikejima K, Morinaga M, Kusama H, Arai K, Aoyama T, Uchiyama A, Yamashina S, and Watanabe S**. L-carnitine prevents metabolic steatohepatitis in obese diabetic KK-A(y) mice. *Hepatol Res* 47: E44-e54, 2017.

29. **Kon K, Ikejima K, Okumura K, Arai K, Aoyama T, and Watanabe S**. Diabetic KK-A(y) mice are highly susceptible to oxidative hepatocellular damage induced by acetaminophen. *Am J Physiol Gastrointest Liver Physiol* 299: G329-337, 2010.

30. **Kono H, Bradford BU, Yin M, Sulik KK, Koop DR, Peters JM, Gonzalez FJ, McDonald T, Dikalova A, Kadiiska MB, Mason RP, and Thurman RG**. CYP2E1 is not involved in early alcohol-induced liver injury. *Am J Physiol* 277: G1259-1267, 1999.

31. **Kono H, Rusyn I, Yin M, Gäbele E, Yamashina S, Dikalova A, Kadiiska MB, Connor HD, Mason RP, and Segal BH**. NADPH oxidase–derived free radicals are key oxidants in alcohol-induced liver disease. *The Journal of clinical investigation* 106: 867-872, 2000.

32. **Koop DR, Klopfenstein B, Iimuro Y, and Thurman RG**. Gadolinium

chloride blocks alcohol-dependent liver toxicity in rats treated chronically with intragastric alcohol despite the induction of CYP2E1. *Mol Pharmacol* 51: 944-950, 1997.

33. **Leclercq S, Matamoros S, Cani PD, Neyrinck AM, Jamar F, Starkel P, Windey K, Tremaroli V, Backhed F, Verbeke K, de Timary P, and Delzenne NM**. Intestinal permeability, gut-bacterial dysbiosis, and behavioral markers of alcohol-dependence severity. *Proc Natl Acad Sci U S A* 111: E4485-4493, 2014.

34. **Levin I, Petrasek J, and Szabo G**. The presence of p47phox in liver parenchymal cells is a key mediator in the pathogenesis of alcoholic liver steatosis. *Alcoholism: Clinical and Experimental Research* 36: 1397-1406, 2012.

35. **Ley RE, Turnbaugh PJ, Klein S, and Gordon JI**. Microbial ecology: human gut microbes associated with obesity. *Nature* 444: 1022-1023, 2006.

36. **Lucey MR, Mathurin P, and Morgan TR**. Alcoholic hepatitis. *N Engl J Med* 360: 2758-2769, 2009.

37. **Magnusson KR, Hauck L, Jeffrey BM, Elias V, Humphrey A, Nath R, Perrone A, and Bermudez LE**. Relationships between diet-related changes in the gut microbiome and cognitive flexibility. *Neuroscience* 300: 128-140, 2015.

38. **Mandrekar P, and Szabo G**. Signalling pathways in alcohol-induced liver

568 inflammation. *J Hepatol* 50: 1258-1266, 2009.

569 39. **Mathurin P, and Lucey MR**. Management of alcoholic hepatitis. *J Hepatol* 56

570 Suppl 1: S39-45, 2012.

571 40. **Miyake Y, and Yamamoto K**. Role of gut microbiota in liver diseases.

572 *Hepatol Res* 43: 139-146, 2013.

573 41. **Mutlu E, Keshavarzian A, Engen P, Forsyth CB, Sikaroodi M, and Gillevet**

574 **P**. Intestinal dysbiosis: a possible mechanism of alcohol-induced endotoxemia and

575 alcoholic steatohepatitis in rats. *Alcohol Clin Exp Res* 33: 1836-1846, 2009.

576 42. **Mutlu EA, Gillevet PM, Rangwala H, Sikaroodi M, Naqvi A, Engen PA,**

577 **Kwasny M, Lau CK, and Keshavarzian A**. Colonic microbiome is altered in

578 alcoholism. *Am J Physiol Gastrointest Liver Physiol* 302: G966-978, 2012.

579 43. **Nanji AA, Khettry U, and Sadrzadeh SM**. Lactobacillus feeding reduces

580 endotoxemia and severity of experimental alcoholic liver (disease). *Proc Soc Exp Biol*

581 *Med* 205: 243-247, 1994.

582 44. **Naveau S, Giraud V, Borotto E, Aubert A, Capron F, and Chaput JC**.

583 Excess weight risk factor for alcoholic liver disease. *Hepatology* 25: 108-111, 1997.

584 45. **O'Neill S, and O'Driscoll L**. Metabolic syndrome: a closer look at the

585 growing epidemic and its associated pathologies. *Obes Rev* 16: 1-12, 2015.

586 46. **Peng JH, Cui T, Huang F, Chen L, Zhao Y, Xu L, Xu LL, Feng Q, and Hu**
587 **YY**. Puerarin ameliorates experimental alcoholic liver injury by inhibition of endotoxin
588 gut leakage, Kupffer cell activation, and endotoxin receptors expression. *J Pharmacol*
589 *Exp Ther* 344: 646-654, 2013.
590 47. **Petrasek J, Csak T, and Szabo G**. Toll-like receptors in liver disease. *Adv*
591 *Clin Chem* 59: 155-201, 2013.
592 48. **Raby AC, Holst B, Le Bouder E, Diaz C, Ferran E, Conraux L, Guillemot**
593 **JC, Coles B, Kift-Morgan A, Colmont CS, Szakmany T, Ferrara P, Hall JE, Topley**
594 **N, and Labeta MO**. Targeting the TLR co-receptor CD14 with TLR2-derived peptides
595 modulates immune responses to pathogens. *Sci Transl Med* 5: 185ra164, 2013.
596 49. **Raff EJ, Kakati D, Bloomer JR, Shoreibah M, Rasheed K, and Singal AK**.
597 Diabetes Mellitus Predicts Occurrence of Cirrhosis and Hepatocellular Cancer in
598 Alcoholic Liver and Non-alcoholic Fatty Liver Diseases. *J Clin Transl Hepatol* 3: 9-16,
599 2015.
600 50. **Roh YS, Zhang B, Loomba R, and Seki E**. TLR2 and TLR9 contribute to
601 alcohol-mediated liver injury through induction of CXCL1 and neutrophil infiltration.
602 *Am J Physiol Gastrointest Liver Physiol* 309: G30-41, 2015.
603 51. **Ronis MJ, Huang J, Crouch J, Mercado C, Irby D, Valentine CR,**

Lumpkin CK, Ingelman-Sundberg M, and Badger TM. Cytochrome P450 CYP 2E1 induction during chronic alcohol exposure occurs by a two-step mechanism associated with blood alcohol concentrations in rats. *J Pharmacol Exp Ther* 264: 944-950, 1993.

52. **Schwab C, Berry D, Rauch I, Rennisch I, Ramesmayer J, Hainzl E, Heider S, Decker T, Kenner L, Muller M, Strobl B, Wagner M, Schleper C, Loy A, and Urich T**. Longitudinal study of murine microbiota activity and interactions with the host during acute inflammation and recovery. *Isme j* 8: 1101-1114, 2014.

53. **Sugimoto K, and Takei Y**. Pathogenesis of alcoholic liver disease. *Hepatol Res* 47: 70-79, 2017.

54. **Suzuki M, Kon K, Ikejima K, Arai K, Uchiyama A, Aoyama T, Yamashina S, Ueno T, and Watanabe S**. The Chemical Chaperone 4-Phenylbutyric Acid Prevents Alcohol-Induced Liver Injury in Obese KK-A(y) Mice. *Alcohol Clin Exp Res* 43: 617-627, 2019.

55. **Takashima S, Ikejima K, Arai K, Yokokawa J, Kon K, Yamashina S, and Watanabe S**. Glycine prevents metabolic steatohepatitis in diabetic KK-Ay mice through modulation of hepatic innate immunity. *Am J Physiol Gastrointest Liver Physiol* 311: G1105-g1113, 2016.

56. **Takeuchi O, Hoshino K, Kawai T, Sanjo H, Takada H, Ogawa T, Takeda K,**

622 **and Akira S**. Differential roles of TLR2 and TLR4 in recognition of gram-negative and
623 gram-positive bacterial cell wall components. *Immunity* 11: 443-451, 1999.

624 57. **Thakur V, Pritchard MT, McMullen MR, Wang Q, and Nagy LE**. Chronic
625 ethanol feeding increases activation of NADPH oxidase by lipopolysaccharide in rat
626 Kupffer cells: role of increased reactive oxygen in LPS - stimulated ERK1/2 activation
627 and TNF - α production. *J Leukoc Biol* 79: 1348-1356, 2006.

628 58. **Turnbaugh PJ, Ley RE, Mahowald MA, Magrini V, Mardis ER, and**
629 **Gordon JI**. An obesity-associated gut microbiome with increased capacity for energy
630 harvest. *Nature* 444: 1027-1031, 2006.

631 59. **Uesugi T, Froh M, Arteel GE, Bradford BU, and Thurman RG**. Toll-like
632 receptor 4 is involved in the mechanism of early alcohol-induced liver injury in mice.
633 *Hepatology* 34: 101-108, 2001.

634 60. **Vassallo G, Mirijello A, Ferrulli A, Antonelli M, Landolfi R, Gasbarrini A,**
635 **and Addolorato G**. alcohol and gut microbiota - the possible role of gut microbiota
636 modulation in the treatment of alcoholic liver disease. *Aliment Pharmacol Ther* 41:
637 917-927, 2015.

638 61. **Vlachogiannakos J, Viazis N, Vasianopoulou P, Vafiadis I, Karamanolis**
639 **DG, and Ladas SD**. Long-term administration of rifaximin improves the prognosis of

patients with decompensated alcoholic cirrhosis. *J Gastroenterol Hepatol* 28: 450-455, 2013.

62. **Yamagata H, Ikejima K, Takeda K, Aoyama T, Kon K, Okumura K, and Watanabe S**. Altered expression and function of hepatic natural killer T cells in obese and diabetic KK-A(y) mice. *Hepatol Res* 43: 276-288, 2013.

63. **Yan AW, Fouts DE, Brandl J, Starkel P, Torralba M, Schott E, Tsukamoto H, Nelson KE, Brenner DA, and Schnabl B**. Enteric dysbiosis associated with a mouse model of alcoholic liver disease. *Hepatology* 53: 96-105, 2011.

Fig. 1. Rifaximin ameliorates hepatic steatosis and inflammation caused by chronic-binge EtOH feeding.

KK-A^y mice were fed a liquid diet containing EtOH (5%) or control diet for 10 days. Some mice were given rifaximin (RFX; 0.1 g/L) in the liquid diet during the feeding period. Mice were then given single EtOH (4 g/kg BW) gavage on day 11, and euthanized 6 h later. Average food consumption (*A*), and changes in body weight are plotted (*B*). Serum alanine aminotransferase (ALT) (*C*) and triglyceride (TG) levels (*D*) are plotted. Macroscopic images of entire livers of each group are shown (*E*). Average values of liver/body weight ratio are plotted (*F*). (n = 5, *; vs. control, #; vs. EtOH, $P <$ 0.05 by ANOVA on ranks and Student–Neuman–Keuls post-hoc test). Error bars represent mean ± SEM.

Fig. 2. Rifaximin ameliorates hepatic steatosis caused by chronic-binge EtOH feeding through by inhibition of lipogenesis.

The experimental design is the same as in Fig. 1. Representative photomicrographs of H-E stained (upper panels) and Oil Red O-stained (lower panels) sections of liver from each group are shown (*A*; original magnification: ×100, scale bar: 100 μm). Hepatic contents of triglyceride (TG) were measured by colorimetric assay. Obtained values were normalized by tissue weight, and average values are plotted (*B*). Hepatic mRNA expression levels of acetyl-CoA carboxylase α (AACα) (*C*), fatty acid synthase (FAS) (*D*), and carnitine palmitoyltransferase 1A (CPT1A) were quantitatively detected by realtime RT-PCR ($n = 5$, *; vs. control, #; vs. EtOH, $P < 0.05$ by ANOVA on ranks and Student–Neuman–Keuls post-hoc test). Error bars represent mean ± SEM.

Fig. 3. Rifaximin decreases overexpression of inflammatory cytokines in the liver in chronic-binge EtOH-fed mice.

Experimental design is the same as in Fig.1 except that mice in Fig. 3I were euthanized 2 h later a single EtOH + D-xylose gavage. Hepatic mRNA expression levels of tumor necrosis factor α (TNFα) (*A*), interleukin 6 (IL6) (*B*), interferon γ (IFNγ) (*C*), C-C motif chemokine ligand 2 (CCL2) (*D*), cluster of differentiation (CD)-14 (*E*), toll-like receptor (TLR) 4 (*F*), and TLR2 (*G*) were quantitatively detected by realtime RT-PCR. Lipopolysaccharide (LPS) in portal blood was measured using limulus amebocyte lysate assay and the average values were plotted (*H*). The intestinal permeability based on D-xylose absorption was plotted (*I*) (n = 5, *; vs. control, #; vs. EtOH, $P < 0.05$ by ANOVA on ranks and Student–Neuman–Keuls post-hoc test). Error bars represent mean ± SEM.

Fig. 4. Rifaximin prevents oxidative stress induced by chronic-binge EtOH.

Experimental design is the same as in Fig.1. Representative photomicrographs of the 4-hydroxy-2-nonenal (4-HNE) stained liver tissues from each group are shown (Fig. 4A; original magnification: ×100, scale bar: 100 μm). The 4-HNE-positive area in the field was measured morphometrically, and average percentages of 4-HNE-positive area from 5 different animals are plotted. Five fields per animal were measured (*B*). Hepatic expression of mRNA for heme oxygenase 1 (HO1) (*C*), NADPH oxidase 1 (NOX1) (*D)*, and NOX2 (*E*) was determined by RT-PCR. Hepatic expression of anti-cytochrome P450 (CYP) 2E1 was detected by Western blotting (*F*). CYP2E1 activity in liver was determined by monitoring the formation of para-nitro-catechol from para-nitro-phenol. The average of para-nitro-catechol concentration increase per minute was plotted. (*G*; $n = 5$, *; vs. control, #; vs. EtOH, $P < 0.05$ by ANOVA on ranks and Student–Neuman–Keuls post-hoc test). Error bars represent mean ± SEM.

Fig. 5. Rifaximin has no effect on the net amount of viable bacterial cells increased by chronic EtOH feeding.

Experimental design is the same as in Fig.1, except that small intestinal contents were collected prior to a single EtOH gavage. Viable bacterial cells were measured by colony forming units (CFU) counted on aerobic culture plate (*A*) or anaerobic culture plate (*B*; $n = 5$, *; vs. control, #; vs. EtOH, $P < 0.05$ by ANOVA on ranks and Student–Neuman–Keuls post-hoc test). Error bars represent mean ± SEM.

Fig. 6. Rifaximin induces taxonomic shifts in small intestinal bacterial communities in chronic EtOH-fed mice.

Experimental design is the same as in Fig.5. Taxonomic composition of the small intestinal bacterial communities in the phylum level (*A*) and the order level (*B*). Relative abundance of *Lactobacillales* (*C*), *Erysipelotrichales* (*D*) and *Bacteroidales* (*E*) in small intestinal microbiota at the order level (n = 3, *; vs. control, #; vs. EtOH, $P < 0.05$ by ANOVA on ranks and Student–Neuman–Keuls post-hoc test). Error bars represent mean ± SEM.

717 **Table 1.** Primer sequences for the targeted mouse genes (RT-PCR assay)
718

719

Primer set	Forward	Reverse
ACCα	GAAGTCAGAGCCACGGCACA	GGCAATCTCAGTTCAAGCCAGTC
CCL2	GCATCCACGTGITGGCTCA	CTCCAGCCTACTCAITGGGATCA
CD-14	CCTGGCACAGAATGCCCTAA	CCTCTGTGAATTCTAAITGCGTCTC
FAS	AGCACTGCCTTCGGTTCAGTC	AAGAGCTGTGGAGGCCACTTG
GAPDH	TGTGTCCGTCGTGGATCTGA	ITGCTGITGAAGTCGCAGGAG
HO1	CTGGAGATGACACCTGAGGTCAA	CTGACGAAGTGACGCCATCTG
IFNy	CGGCACAGTCAITGAAAGCCTA	GITGCTGATGGCCTGATTGTC
IL6	CCACTTCACAAGTCGGAGGCTTA	GCAAGTGCATCATCGITGITCATAC
NOX1	AAGCCATTGGATCACAACCTCAC	ATCCATGGCCTGTTGGCTTC
NOX2	CCTTAGAGCACTCAAGGCTGGTTC	CTTTGTCCCAGGGCAACAATTC
TLR2	GGACGTITGCTATGATGCCTITG	ACGAAGTCCCGCTTGTGGAG
TLR4	TCCTGTGGACAAGGTCAGCAAC	TTACACTCAGACTCGGCACTTAGCA
TNFα	GTTCTATGGCCCAGACCCTCAC	GGCACCACTAGITGGITGTCTITG

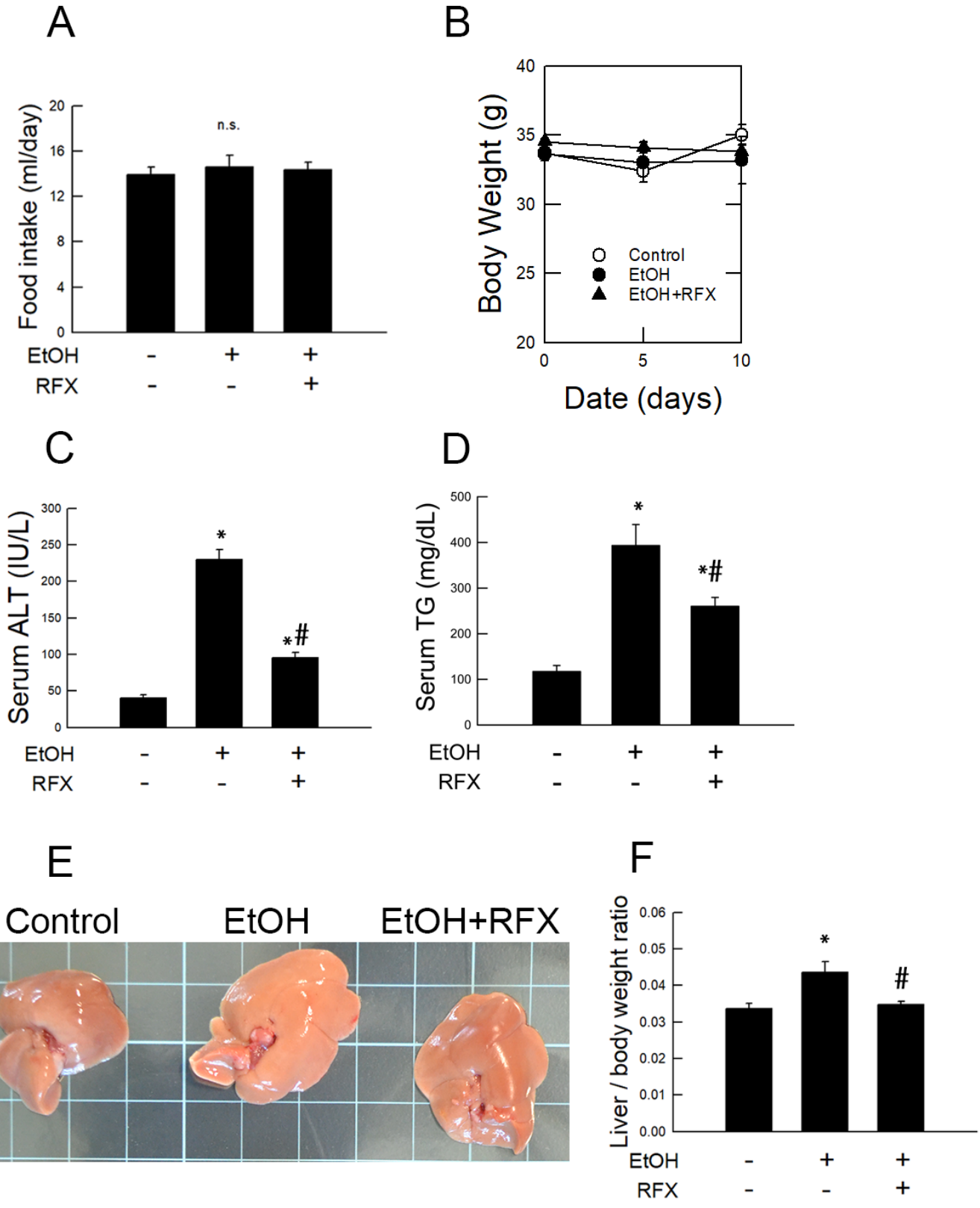
A
Food intake (ml/day)
20
16
12
8
4
0
n.s.
EtOH - + +
RFX - - +
B
Body Weight (g)
40
35
30
25
20
0
5
10
Date (days)
Control
EtOH
EtOH+RFX
C
Serum ALT (IU/L)
300
250
200
150
100
50
0
*
*#
EtOH - + +
RFX - - +
D
Serum TG (mg/dL)
500
400
300
200
100
0
*
*#
EtOH - + +
RFX - - +
E
Control
EtOH
EtOH+RFX
F
Liver / body weight ratio
0.06
0.05
0.04
0.03
0.02
0.01
0.00
*
#
EtOH - + +
RFX - - +

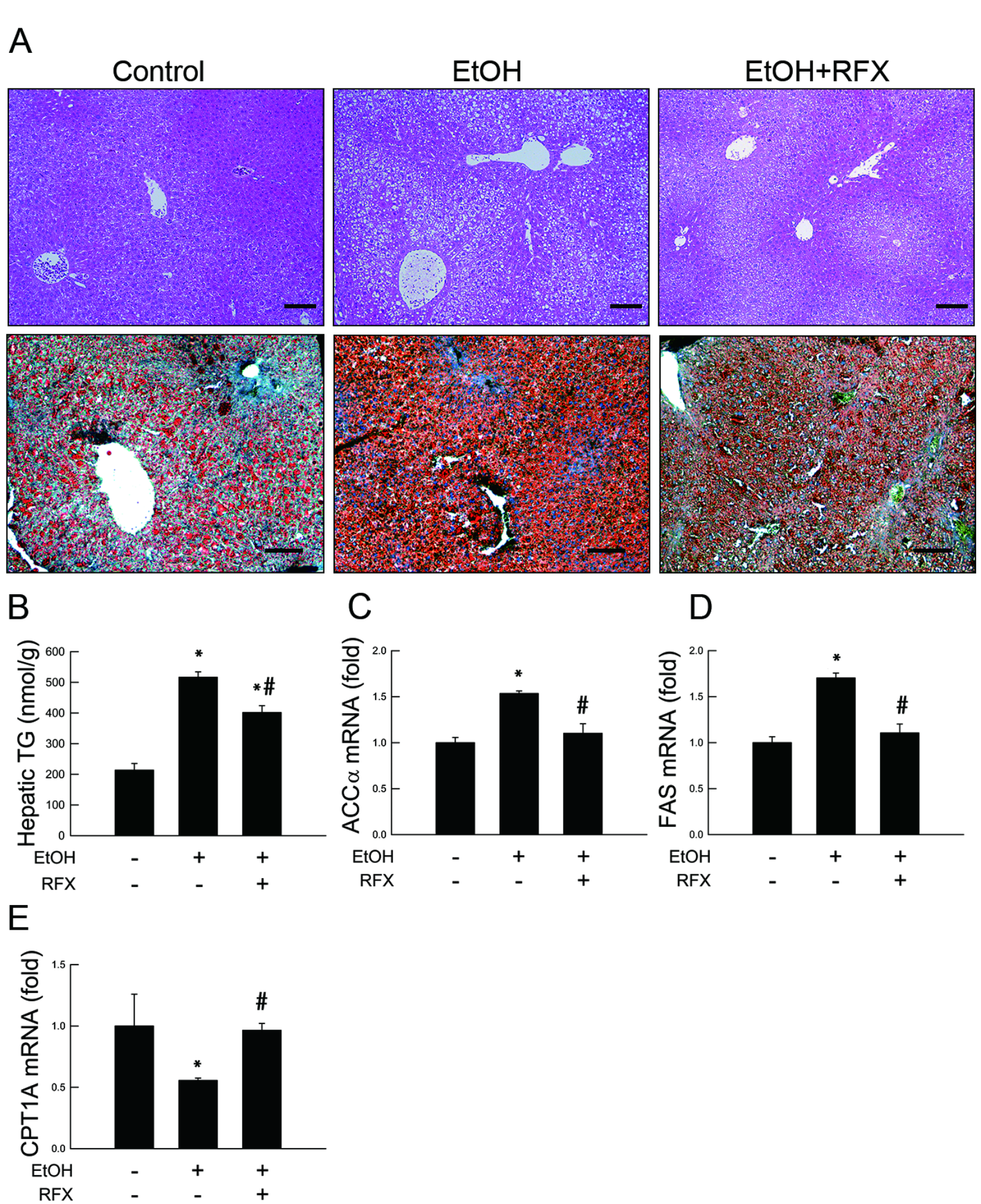
A
Control
EtOH
EtOH+RFX
B
Hepatic TG (nmol/g)
600
500
400
300
200
100
0
*
*#
EtOH - + +
RFX - - +
C
ACCα mRNA (fold)
2.0
1.5
1.0
0.5
0.0
*
#
EtOH - + +
RFX - - +
D
FAS mRNA (fold)
2.0
1.5
1.0
0.5
0.0
*
#
EtOH - + +
RFX - - +
E
CPT1A mRNA (fold)
1.5
1.0
0.5
0.0
*
#
EtOH - + +
RFX - - +

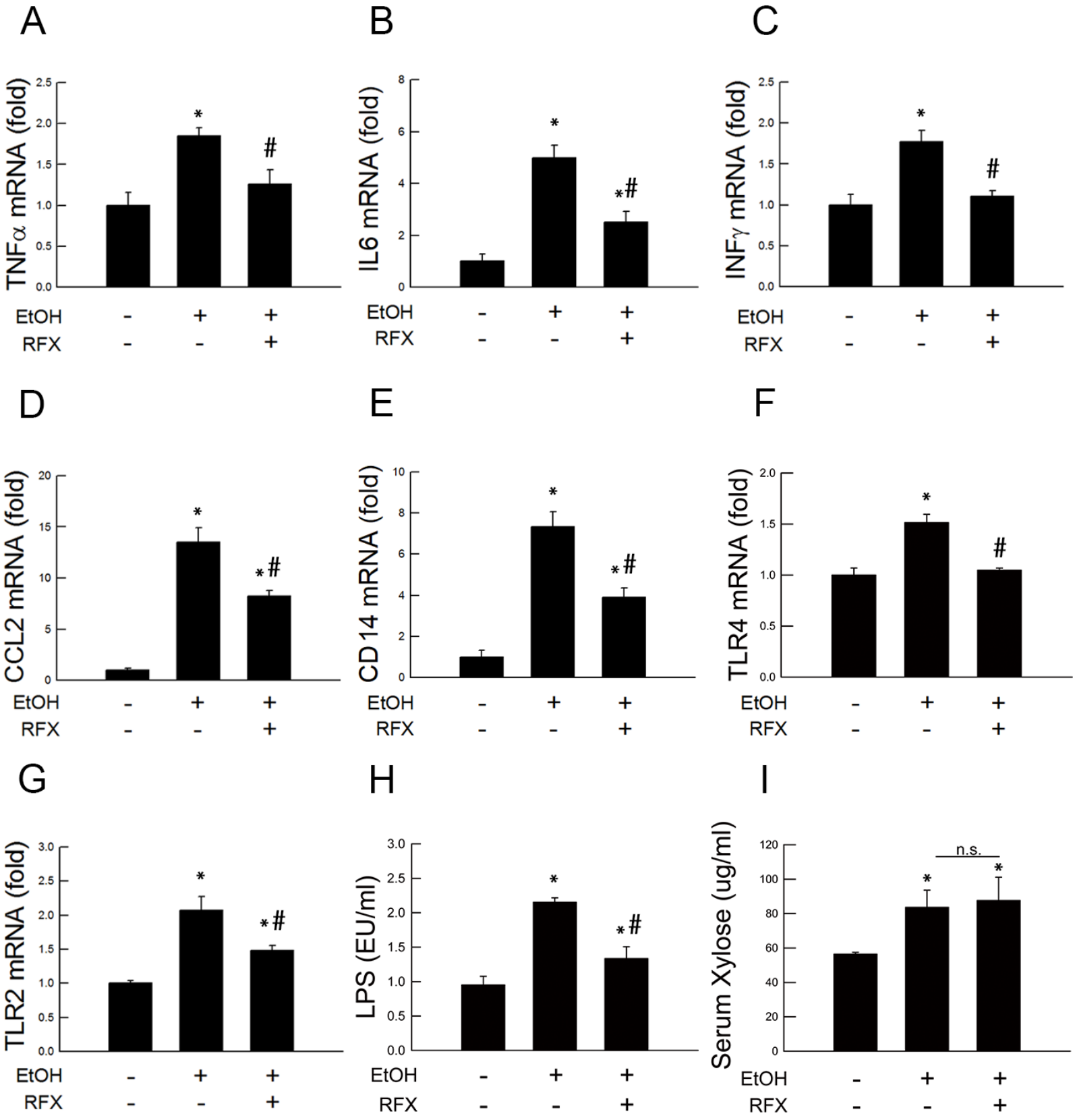
A
TNFα mRNA (fold)
2.5
2.0
1.5
1.0
0.5
0.0
*
#
EtOH - + +
RFX - - +
B
IL6 mRNA (fold)
8
6
4
2
0
*
*#
EtOH - + +
RFX - - +
C
INFγ mRNA (fold)
2.5
2.0
1.5
1.0
0.5
0.0
*
#
EtOH - + +
RFX - - +
D
CCL2 mRNA (fold)
20
15
10
5
0
*
*#
EtOH - + +
RFX - - +
E
CD 14 mRNA (fold)
10
8
6
4
2
0
*
*#
EtOH - + +
RFX - - +
F
TLR4 mRNA (fold)
2.0
1.5
1.0
0.5
0.0
*
#
EtOH - + +
RFX - - +
G
TLR2 mRNA (fold)
3.0
2.5
2.0
1.5
1.0
0.5
0.0
*
*#
EtOH - + +
RFX - - +
H
LPS (EU/ml)
3.0
2.5
2.0
1.5
1.0
0.5
0.0
*
*#
EtOH - + +
RFX - - +
I
Serum Xylose (ug/ml)
120
100
80
60
40
20
0
n.s.
*
*
EtOH - + +
RFX - - +

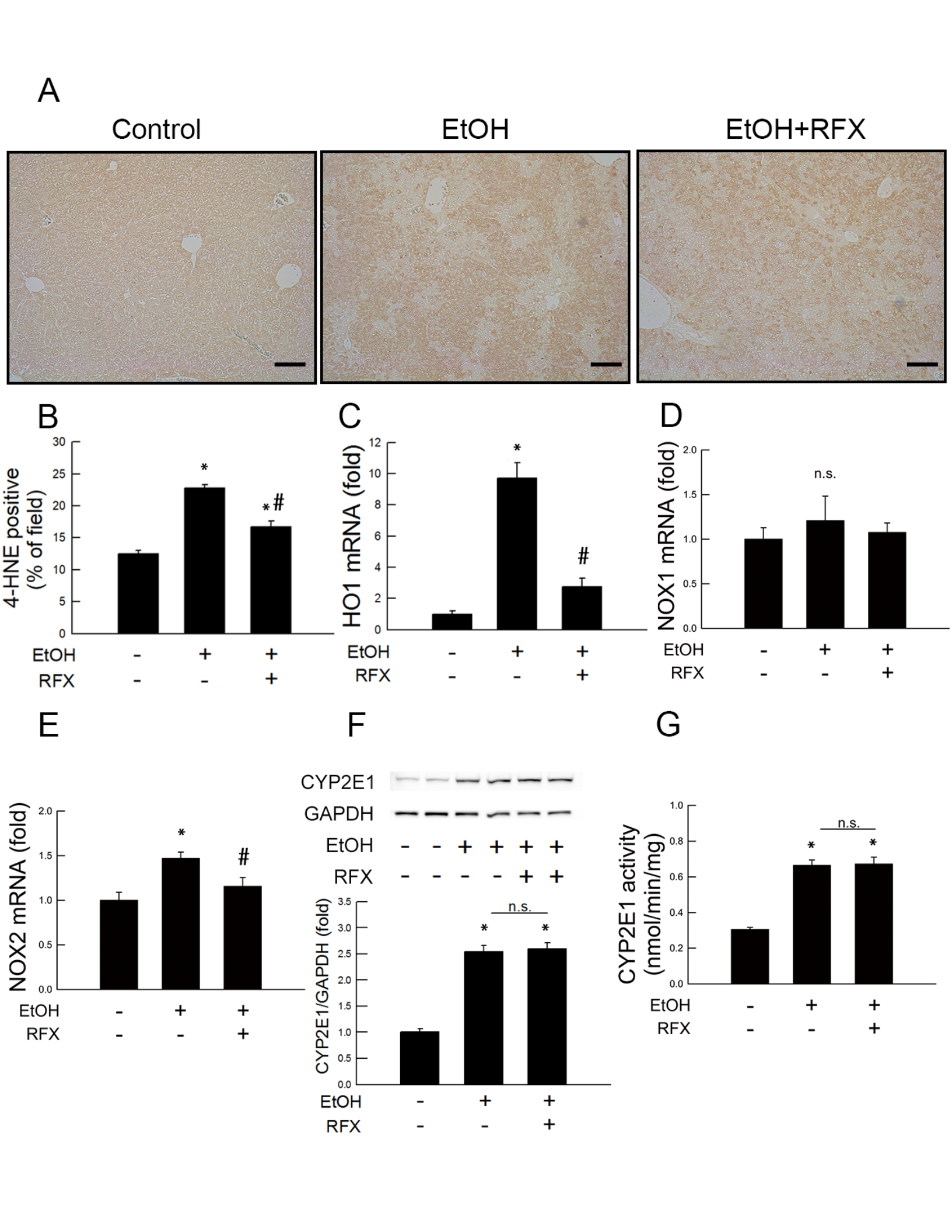
A
Control
EtOH
EtOH+RFX
B
4-HNE positive (% of field)
30
25
20
15
10
5
0
*
*#
EtOH - + +
RFX - - +
C
HO1 mRNA (fold)
12
10
8
6
4
2
0
*
#
EtOH - + +
RFX - - +
D
NOX1 mRNA (fold)
2.0
1.5
1.0
0.5
0.0
n.s.
EtOH - + +
RFX - - +
E
NOX2 mRNA (fold)
2.0
1.5
1.0
0.5
0.0
*
#
EtOH - + +
RFX - - +
F
CYP2E1
GAPDH
EtOH - - + + + +
RFX - - - - + +
CYP2E1/GAPDH (fold)
3.5
3.0
2.5
2.0
1.5
1.0
0.5
0.0
n.s.
*
*
EtOH - + +
RFX - - +
G
CYP2E1 activity (nmol/min/mg)
1.0
0.8
0.6
0.4
0.2
0.0
n.s.
*
*
EtOH - + +
RFX - - +

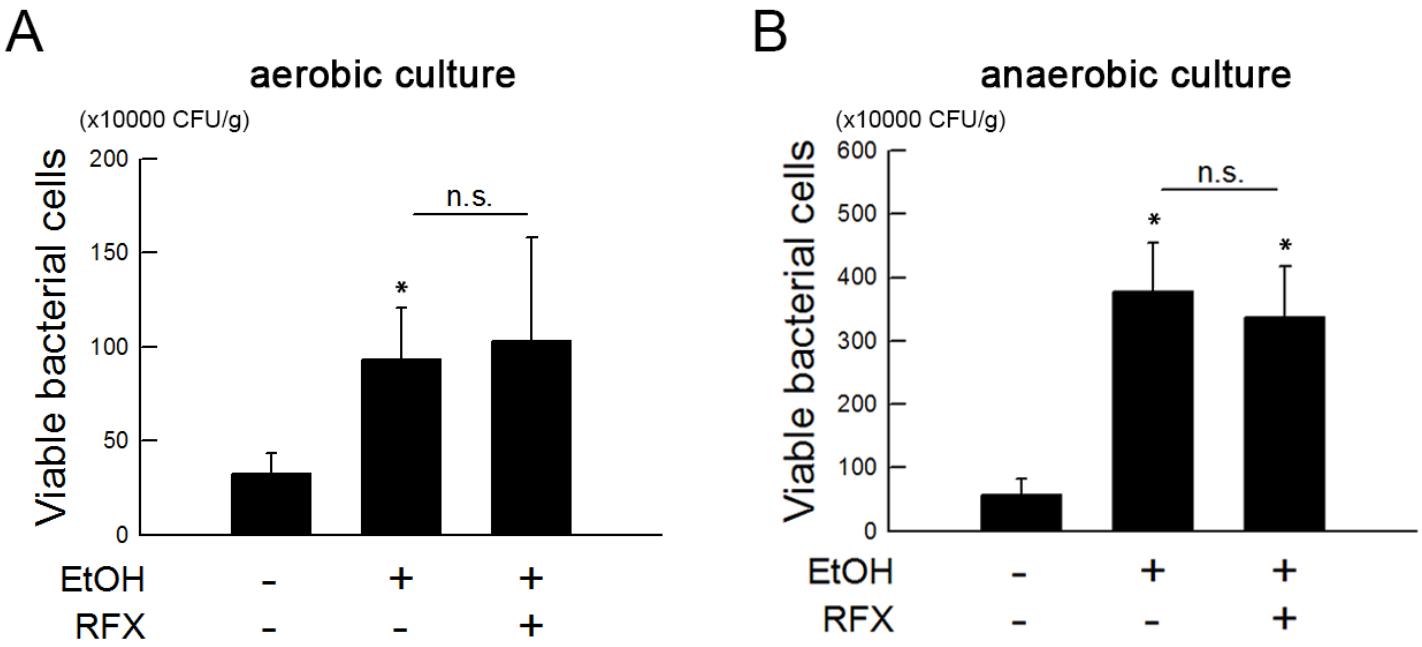
A
aerobic culture
(x10000 CFU/g)
Viable bacterial cells
200
150
100
50
0
n.s.
*
EtOH - + +
RFX - - +
B
anaerobic culture
(x10000 CFU/g)
Viable bacterial cells
600
500
400
300
200
100
0
n.s.
*
*
EtOH - + +
RFX - - +

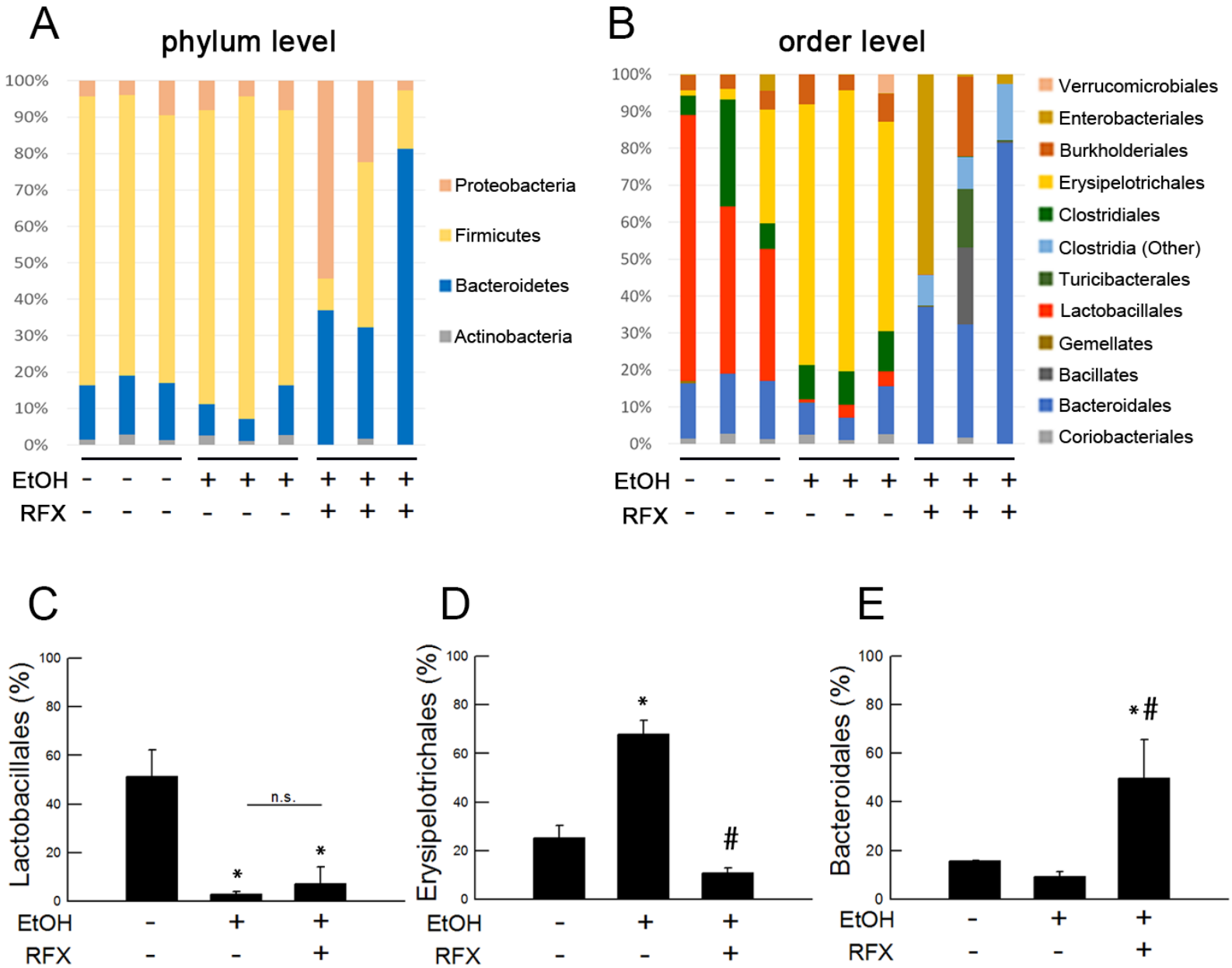
A
phylum level
100%
90%
80%
70%
60%
50%
40%
30%
20%
10%
0%
Proteobacteria
Firmicutes
Bacteroidetes
Actinobacteria
EtOH - - - + + + + + +
RFX - - - - - - + + +
B
order level
Verrucomicrobiales
Enterobacteriales
Burkholderiales
Erysipelotrichales
Clostridiales
Clostridia (Other)
Turicibacterales
Lactobacillales
Gemellates
Bacillates
Bacteroidales
Coriobacteriales
EtOH - - - + + + + + +
RFX - - - - - - + + +
C
Lactobacillales (%)
n.s.
*
*
EtOH - + +
RFX - - +
D
Erysipelotrichales (%)
*
#
EtOH - + +
RFX - - +
E
Bacteroidales (%)
*#
EtOH - + +
RFX - - +

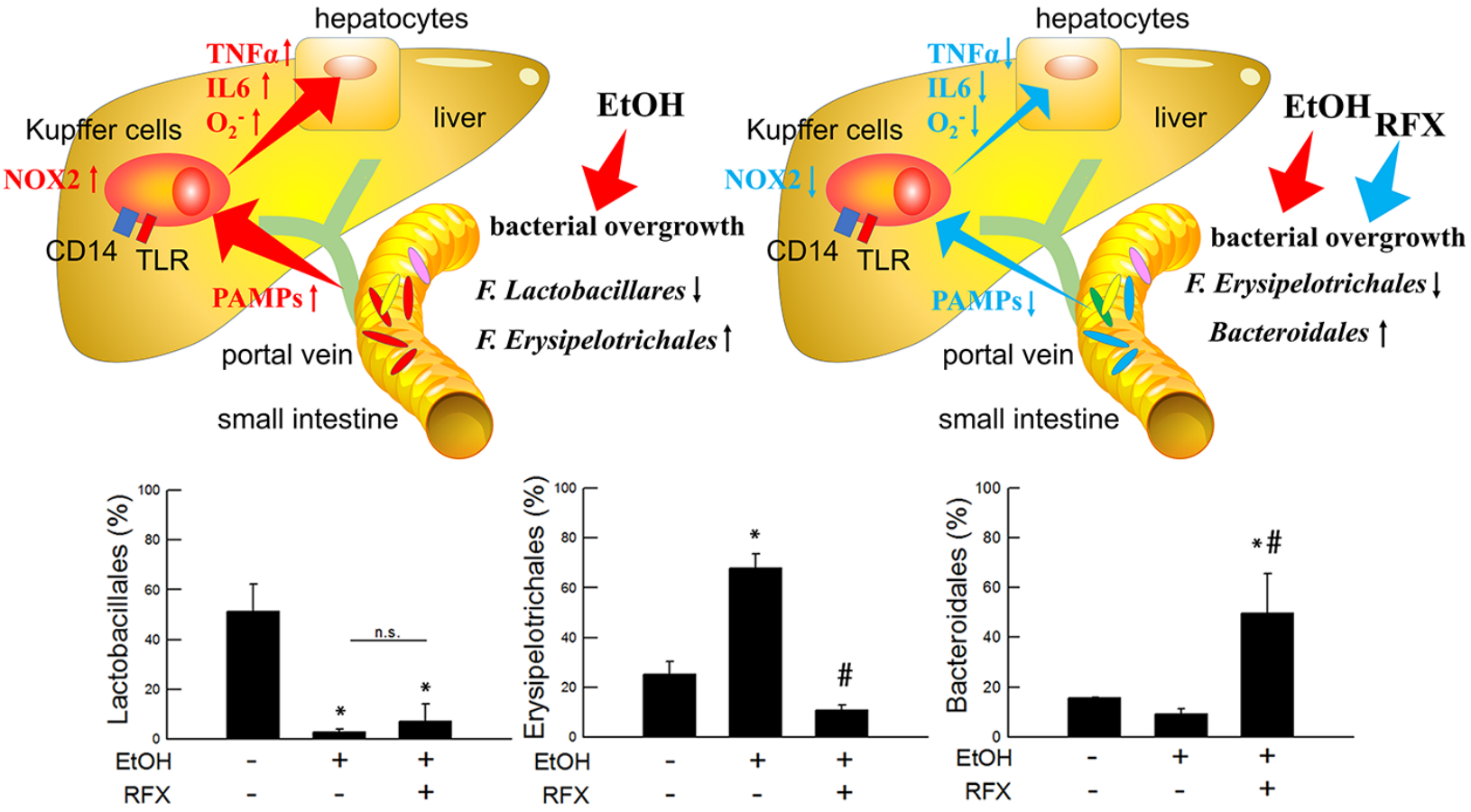
hepatocytes
TNFα↑
IL6↑
O2-↑
Kupffer cells
liver
NOX2↑
CD14
TLR
PAMPs↑
EtOH
bacterial overgrowth
F. Lactobacillares↓
F. Erysipelotrichales↑
portal vein
small intestine
hepatocytes
TNFα↓
IL6↓
O2-↓
Kupffer cells
liver
NOX2↓
CD14
TLR
PAMPs↓
EtOH
RFX
bacterial overgrowth
F. Erysipelotrichales↓
Bacteroidales↑
portal vein
small intestine
Lactobacillales (%)
n.s.
EtOH
RFX
Erysipelotrichales (%)
EtOH
RFX
Bacteroidales (%)
EtOH
RFX